Moyle et al., http://www.jcb.org/cgi/content/full/jcb.201311015/DC1

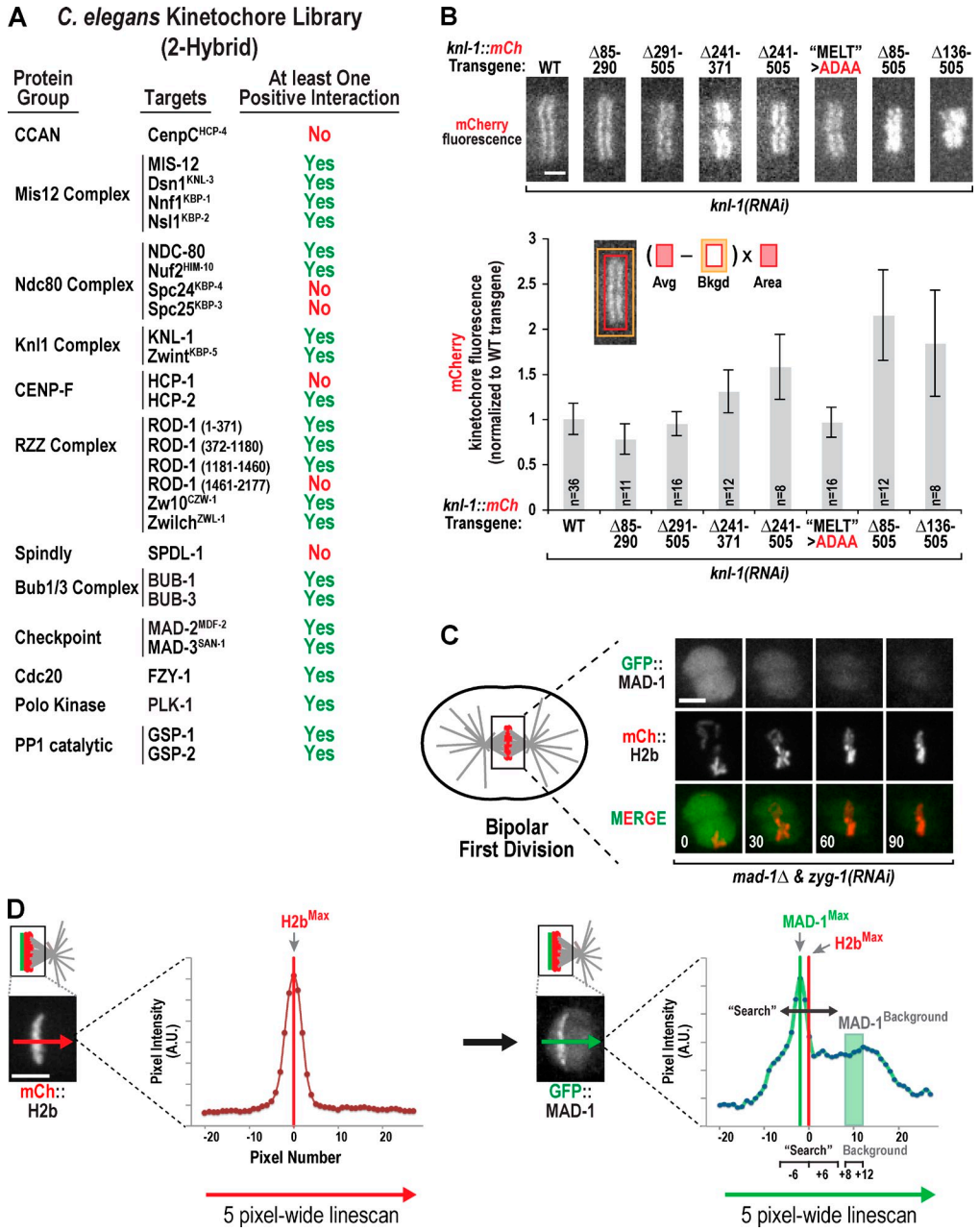

Figure S1. **Yeast two-hybrid library, analysis of KNL-1 variant expression, MAD-1 localization during bipolar mitosis, and method for quantifying MAD-1 localization at unattached kinetochores.** (A) *C. elegans* kinetochore protein library. Tested targets that exhibit at least one positive interaction with another tested target protein are marked with a Yes (e.g., GSP-1/2 with KNL-1 [Espeut et al., 2012]; ROD-1 [aa 1–371] with NDC-80 [Cheerambathur et al., 2013]), indicating that they are expressed at a sufficient level in yeast to enable detection of a positive interaction. The six components that to date have not exhibited any positive interactions are marked with a No and could represent false negatives as a result of problems with expression/stability of the fusions in yeast. (B) Expression of KNL-1::mCh variants monitored by measuring integrated kinetochore fluorescence after background subtraction (see schematic for method). Endogenous KNL-1 was depleted; the transgene-encoded KNL-1 variants are RNAi resistant (Espeut et al., 2012). The WT image is the same as in Fig. 2 B. Error bars are 95% confidence interval of the mean. Avg, average; Bkgd, background. (C) GFP::MAD-1 localization on bipolar spindles. A one-cell embryo depleted of ZYG-1 is shown. As sperm bring in two centrioles, the first division in a ZYG-1–depleted embryo is bipolar, and the next division is monopolar (O'Connell et al., 2001; Essex et al., 2009). Time (in seconds) is on the bottom left of merge images and is relative to NEBD. (D) Method used to quantify localization of GFP::MAD-1 (WT and engineered variants) to unattached kinetochores of monopolar spindles (Fig. 2, A and D; Fig. 4 C; and Fig. 5 D). The time point chosen for analysis was pseudometaphase plate formation on the monopolar spindles (see Materials and methods). Monopolar spindles were oriented with their single pole on the right and a 5-pixel-wide line scan was drawn at the same image position in the mCh::H2b and GFP::MAD-1 channels. The peak of H2b::mCh fluorescence was used to define pixel 0. In the GFP::MAD-1 line scan, 6-pixel-wide regions on either side of pixel 0 were searched to identify the peak MAD-1 signal (MAD-1^{Max}). Because of the asymmetric "cloud" of nonkinetochore signal, background estimation was performed by averaging the pixel intensities between 8 and 12 pixels (MAD-1^{Background}). The background was subtracted from MAD-1^{Max} and is reported as a measure of the kinetochore-localized signal. This same approach was used for measuring GFP::BUB-1 and KNL-1::mCh (WT and variants) localization to kinetochores of monopolar spindles (Fig. 2, C and D). Videos 1–5 show the entire dynamic localization pattern for the different conditions analyzed; two examples are shown per condition. The images shown are from GFP::MAD-1(WT) Fig. 4 B. A.U., arbitrary unit. Bars: (B) 2 µm; (C and D) 5 µm.

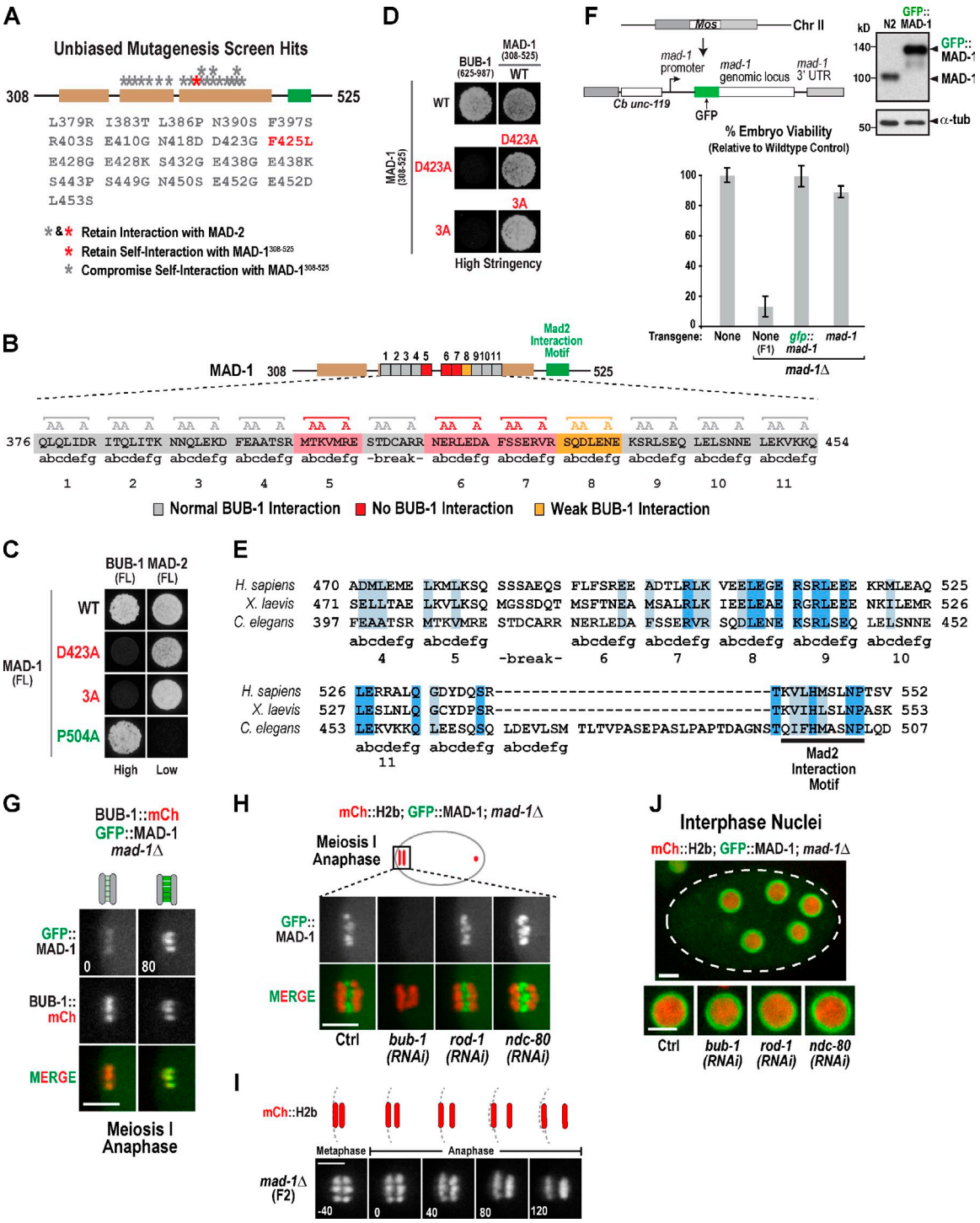

Figure S2. **Hits from unbiased mutagenic yeast two-hybrid, MAD-1 coiled-coil sequence, and MAD-1 localization analysis.** (A) List of mutated residues recovered in the unbiased mutagenic yeast two-hybrid screen. (B) Sequence of coiled-coil region targeted for mutagenesis of predicted b, c, and f residues. The coiled-coil register is predicted with Paircoil2 (McDonnell et al., 2006). (C) Two-hybrid analysis with FL BUB-1 and MAD-1. BUB-1 (FL) exhibits auto-activation in low stringency conditions. Thus, the analysis of BUB-1 (FL)–MAD-1 (FL) interactions was performed under high stringency. (D) MAD-1$^{308–525}$ self-interaction test for 3A and D423A mutants. The analysis was conducted under high stringency conditions. (E) Sequence alignment of coiled-coil region preceding the Mad2 interaction motif. The accession numbers for the human and frog Mad1 sequences are NP_003541 and NP_001080972 (obtained from GenBank). The alignment was generated using T-Coffee in Jalview 2.8 (Notredame et al., 2000; Waterhouse et al., 2009). Light blue, amino acid similarity; dark blue, amino acid identity. (F) Single copy transgene insertion system for *gfp::mad-1*. Anti–MAD-1 immunoblot (top right) and α-tubulin immunoblot (bottom right); α-tubulin (α-tub) serves as a loading control. Chr II, chromosome II. (bottom) Embryo viability analysis for the indicated genotypes. For *mad-1Δ*, the progeny laid by F1 generation homozygotes (derived from a balanced heterozygous parent) were analyzed. Values were normalized relative to the WT (N2) control. At least 6 worms and >260 embryos were counted per condition. Error bars are 95% confidence interval of the mean. (G) Images of early oocyte meiosis I anaphase in a strain expressing GFP::MAD-1 and BUB-1::mCh. The sequence shown is representative of six imaged embryos. The numbers are the times (in seconds) relative to the first image. (H) Images of early oocyte meiosis I anaphase. (top) Region analyzed is described in schematic. Merge is a color overlay of the mCh::H2b and GFP::MAD-1 signals. Images show that this localization depends on BUB-1 ($n = 5$) but not ROD-1 ($n = 6$) or NDC-80 ($n = 5$). The control (Ctrl) and *bub-1(RNAi)* images are reproduced from Fig. 4 F. (I) Images of meiosis I segregation monitored using mCh::H2b in an F2 zygote dissected from an F1 homozygous *mad-1Δ* worm. Time is in seconds relative to anaphase onset. A representative sequence from seven imaged *mad-1Δ* embryos is shown; no significant meiotic missegregation was detected by this assay in the imaged embryos. (J) Images of nuclear periphery enrichment of MAD-1 for the indicated conditions. Dotted line indicates the edge of the multicellular embryo; the embryo shown is the same as in Fig. 4 G. At least seven embryos were imaged per condition, and a representative nucleus for each condition is shown. Bars, 5 µm.

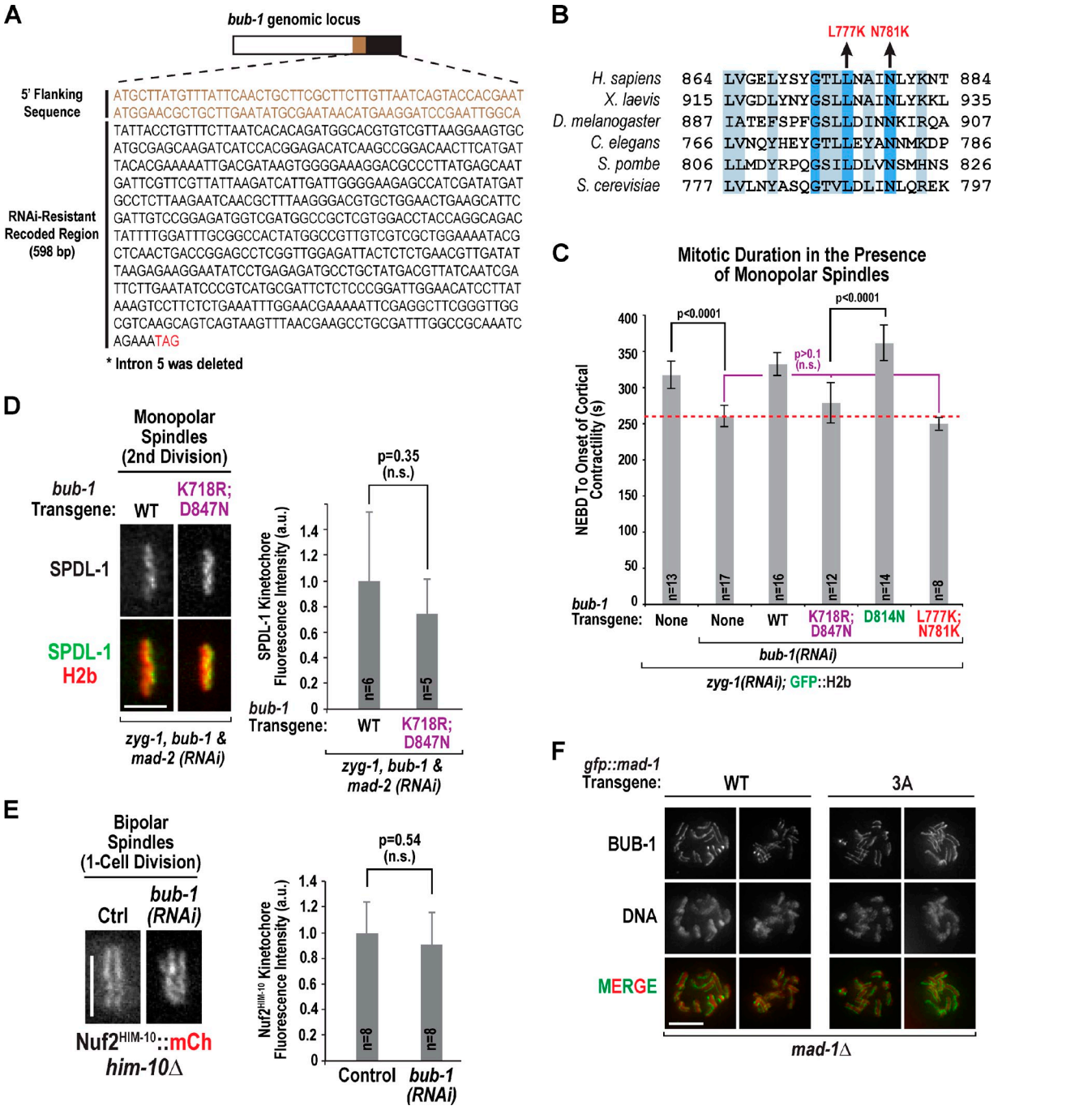

Figure S3. **BUB-1 transgene, checkpoint signaling in BUB-1 mutants, and kinetochore localization analysis of SPDL-1, BUB-1, and NDC-80.** (A) Reencoded nucleotide sequence of *bub-1* that was used to generate the RNAi-resistant *bub-1* transgene. In the transgene, the short (44 bp) intron 5 was deleted. A dsRNA corresponding to the reencoded region was used to deplete endogenous BUB-1 in all RNAi-based replacement experiments. (B) Sequence alignment of the region of BUB-1 harboring the compensatory N781D mutation. The alignment was generated using T-Coffee in Jalview 2.8 (Notredame et al., 2000; Waterhouse et al., 2009). See also Fig. 5 B. The two mutations introduced to disrupt the interaction with MAD-1 are indicated. Light blue, amino acid similarity; dark blue, amino acid identity. (C) Analysis of checkpoint signaling in the presence of monopolar spindles for the indicated conditions. The time from NEBD to onset of cortical contractility was measured. *n* refers to the number of embryos filmed. Error bars represent the 95% confidence interval of the mean. Selected p-values derived from unpaired *t* tests are annotated on the graph. The red dotted line indicates mitotic duration in *bub-1(RNAi)*, where the checkpoint is inactive. (D) Analysis of SPDL-1 localization on monopolar spindles generated by ZYG-1 depletion in the presence of BUB-1 WT or the BUB1 K718R;D847N mutant that prevents MAD-1 localization (Fig. 5 D). SPDL-1::mCh (Cheerambathur et al., 2013; false-colored green in the merge) was crossed into a strain harboring the indicated untagged *bub-1* transgenes and expressing GFP::H2b (false-colored red in the merge). Endogenous BUB-1 was depleted to enable replacement with transgene-encoded versions; MAD-2 was depleted to equalize cell cycle duration for the two compared states, and ZYG-1 was depleted to generate monopolar spindles to assess SPDL-1 localization. Graph on the right shows SPDL-1 fluorescence intensity measured similarly to KNL-1 in Fig. S1 B. *n* is number of embryos imaged, and error bars represent the 95% confidence interval of the mean. The p-value from an unpaired *t* test shows no significant difference. a.u., arbitrary unit. (E) Analysis of Nuf2^{HIM-10} localization to kinetochores in one-cell embryos undergoing bipolar mitosis after BUB-1 depletion. The Nuf2^{HIM-10} transgene rescues the lethal *him-10(ok263)* deletion (referred to as *him-10Δ*), and the localization analysis was conducted in the rescued strain. Depletion of BUB-1, which perturbs chromosome alignment, did not affect Nuf2^{HIM-10} kinetochore localization. Representative metaphase images are shown for a control (Ctrl) and a *bub-1(RNAi)* embryo. Quantification of fluorescence intensity, performed as for KNL-1 in Fig. S1 B, is shown on the right. *n* is number of embryos imaged, and error bars represent the 95% confidence interval of the mean. The p-value from an unpaired *t* test shows no significant difference between control and *bub-1(RNAi)*. (F) Immunofluorescence analysis of BUB-1 localization in the presence of *mad-1^{WT}* and *mad-1^{3A}* transgenes; the endogenous *mad-1* locus is deleted. Two representative prometaphase embryos are shown per condition; no significant defect in BUB-1 localization was observed in *mad-1^{3A}* embryos (*n* = 7) compared with *mad-1^{WT}* embryos (*n* = 20). Bars, 5 µm.

Table S1. ***C. elegans* strains used in this study**

Strain number	Genotype
N2 (ancestral)	
OD56	*unc-119(ed3)III; ltIs37 [pAA64; pie-1/mCHERRY::his-58; unc-119 (+)]IV*
OD738	*mdf-1(gk2) V/nT1(qIs51) (IV;V)*
OD975	*ltSi1[pOD809/pJE110; Pknl-1::KNL-1reencoded::RFP; cb-unc-119(+)]II; unc-119(ed3)?III; ddIs68[bub-1::TY1::EGFP::3×FLAG(92C12)+unc-119(+)]*
OD976	*ltSi44[pOD1039/pJE170; Pknl-1::KNL-1reencoded(Mutant D85–505)::RFP; cb-unc-119(+)]II; unc-119(ed3)?III; ddIs68[bub-1::TY1::EGFP::3×FLAG(92C12)+unc-119(+)]*
OD977	*ltSi23[pOD1011/pJE161; Pknl-1::KNL-1reencoded(Mutant D291–505)::RFP; cb-unc-119(+)]II; unc-119(ed3)?III; ddIs68[bub-1::TY1::EGFP::3×FLAG(92C12)+unc-119(+)]*
OD978	*ltSi23[pOD1011/pJE161; Pknl-1::KNL-1reencoded(Mutant D85–290)::RFP; cb-unc-119(+)]II; unc-119(ed3)?III; ddIs68[bub-1::TY1::EGFP::3×FLAG(92C12)+unc-119(+)]*
OD983	*ltSi260[pTK008 Pknl-1::KNL-1reencoded(Mutant D241–371)::RFP; cb-unc-119(+)]II; unc-119(ed3)?III; ddIs68[bub-1::TY1::EGFP::3×FLAG(92C12)+unc-119(+)]*
OD1015	*ltSi48[pOD1038/pJE169; Pknl-1::KNL-1reencoded(MELT repeats mutant)::RFP; cb-unc-119(+)]II; unc-119(ed3)?III; ddIs68[bub-1::TY1::EGFP::3×FLAG(92C12)+unc-119(+)]*
OD1016	*ltSi261[pTK009 Pknl-1::KNL-1reencoded(Mutant D241–505)::RFP; cb-unc-119(+)]II; unc-119(ed3)?III; ddIs68[bub-1::TY1::EGFP::3×FLAG(92C12)+unc-119(+)]*
OD1051	*ltSi310[pOD1577/pMM7C; Pmdf-1::mdf-1::mdf-1 3′UTR; cb-unc-119(+)]II; unc-119(ed3)?III; mdf-1(gk2)V*
OD1052	*ltSi1[pOD809/pJE110; Pknl-1::KNL-1reencoded::RFP; cb-unc-119(+)]II; unc-119(ed3)?III; unc-46 mdf-1(gk2)V; jzIs1[pRK139; Ppie-1::GFP::mdf-1 unc-119(+)]*
OD1053	*ltSi44[pOD1039/pJE170; Pknl-1::KNL-1reencoded(Mutant D85–505)::RFP; cb-unc-119(+)]II; unc-119(ed3)?III; unc-46 mdf-1(gk2)V; jzIs1[pRK139; Ppie-1::GFP::mdf-1 unc-119(+)]*
OD1075	*ltSi310[pOD1577/pMM7C; Pmdf-1::mdf-1::mdf-1 3′UTR; cb-unc-119(+)]II; unc-119(ed3)?III, ltIs37 [pAA64; pie-1/mCHERRY::his-58; unc-119 (+)]IV; mdf-1(gk2)V*
OD1078	*ltSi264[pTK011; Pbub-1::Bub1 reencoded-RFP; cb-unc-119(+)]II; unc-119(ed3)?III; unc-46 mdf-1(gk2)V; jzIs1[pRK139; Ppie-1::GFP::mdf-1 unc-119(+)]*
OD1120	*ltSi268[pTK013; Pbub-1::Bub1 reencoded; cb-unc-119(+)]II; unc-119(ed3)?III; ruIs32[pAZ132; pie-1/GFP::histone H2B]III; ddIs6 [GFP::tbg-1; unc-119(+)]V*
OD1121	*ltSi270[pOD/pTK014; Pbub-1::Bub1 reencoded(mut K718R, D847N) cb-unc-119(+)]II; unc-119(ed3)?III; ruIs32[pAZ132; pie-1/GFP::histone H2B]III; ddIs6 [GFP::tbg-1; unc-119(+)]V*
OD1161	*unc-119(ed3)?III; ltIs37 [pAA64; pie-1/mCHERRY::his-58; unc-119 (+)]IV; mdf-1(gk2) V/nT1(qIs51) (IV;V)*
OD1208	*ltSi608[pOD1583/pMM30; pmdf-1::GFP::mdf1::mdf-1 3′UTR; cb-unc-119(+)]II; unc-119(ed3)?III; mdf-1(gk2)V*
OD1209	*ltSi608[pOD1583/pMM30; pmdf-1::GFP::mdf1::mdf-1 3′UTR; cb-unc-119(+)]II; unc-119(ed3)?III; ltIs37 [pAA64; pie-1/mCHERRY::his-58; unc-119 (+)]IV; mdf-1(gk2)V*
OD1241	*ltSi378[pTK022 Pknl-1::KNL-1reencoded(Mutant D136–505)::RFP; cb-unc-119(+)]II; unc-119(ed3)?III; ddIs68[bub-1::TY1::EGFP::3×FLAG(92C12)+unc-119(+)]*
OD1262	*ltSi609[pOD1584/pMM9; Pmdf-1::mdf-1(P504A)::mdf-1 3′UTR; cb-unc-119(+)]II;unc-119(ed3)?III; mdf1(gk2)V*
OD1263	*ltSi609[pOD1584/pMM9; Pmdf-1::mdf-1(P504A)::mdf-1 3′UTR; cb-unc-119(+)]II; unc-119(ed3)?III; ltIs37 [pAA64; pie-1/mCHERRY::his-58; unc-119 (+)]IV; mdf-1(gk2)V*
OD1264	*ltSi612[pOD1587/pMM2; pmdf-1::mdf1(D423A)::mdf1 3′UTR; cb-unc-119(+)]II; unc-119(ed3)?III; mdf1(gk2)V*
OD1265	*ltSi612[pOD1587/pMM2; pmdf-1::mdf1(D423A)::mdf1 3′UTR; cb-unc-119(+)]II; unc-119(ed3)?III; ltIs37 [pAA64; pie-1/mCHERRY::his-58; unc-119 (+)]IV; mdf-1(gk2)V*
OD1266	*ltSi611[pOD1586/pMM4; pmdf-1::GFP::mdf1(D423A)::mdf1 3′UTR; cb-unc-119(+)]II; unc-119(ed3)?III; mdf1(gk2)V*
OD1267	*ltSi611[pOD1586/pMM4; pmdf-1::GFP::mdf1(D423A)::mdf1 3′UTR; cb-unc-119(+)]II; unc-119(ed3)?III; ltIs37 [pAA64; pie-1/mCHERRY::his-58; unc-119 (+)]IV; mdf-1(gk2)V*
OD1349	*ltSi617[pOD1592/pMMB1-1; pbub1::bub1 recoded exon5/6::bub1 3′UTR; cb-unc-119(+)]I; unc-119(ed3)III*
OD1357	*ltSi613[pOD1588/pMM7; pmdf-1::GFP::mdf1(P504A)::mdf1 3′UTR; cb-unc-119(+)]II; unc-119(ed3)?III; mdf-1(gk2)V*
OD1358	*ltSi613[pOD1588/pMM7; pmdf-1::GFP::mdf1(P504A)::mdf1 3′UTR; cb-unc-119(+)]II; unc-119(ed3)?III; ltIs37 [pAA64; pie-1/mCHERRY::his-58; unc-119 (+)]IV; mdf-1(gk2)V*
OD1421	*ltSi620[pOD1595/pMM13; pmdf-1::GFP::mdf1(E419A, R420A, D423A)::mdf1 3′UTR; cb-unc-119(+)]II; unc-119(ed3)?III; ltIs37 [pAA64; pie-1/mCHERRY::his-58; unc-119 (+)]IV; mdf-1(gk2)V*
OD1422	*ltSi620[pOD1595/pMM13; pmdf-1::GFP::mdf1(E419A, R420A, D423A)::mdf1 3′UTR; cb-unc-119(+)]II; unc-119(ed3)?III; mdf-1(gk2)V*
OD1429	*ltSi621[pOD1596/pMM20; pmdf-1::mdf1(E419A, R420A, D423A)::mdf1 3′UTR; cb-unc-119(+)]II; unc-119(ed3)?III; ltIs37 [pAA64; pie-1/mCHERRY::his-58; unc-119 (+)]IV; mdf-1(gk2)V*
OD1430	*ltSi621[pOD1596/pMM20; pmdf-1::mdf1(E419A, R420A, D423A)::mdf1 3′UTR; cb-unc-119(+)]II;unc-119(ed3)?III; mdf-1(gk2)V*
OD1449	*ltSi628[pOD1603/pMM2; pbub1::bub1 recoded exon5/6(D814N)::bub1 3′UTR; cb-unc-119(+)]I; unc-119(ed3)III*
OD1452	*ltSi629[pOD1604/pMM27; pbub1::bub1 recoded exon5/6(K718R;D847N)::bub1 3′UTR; cb-unc-119(+)]I; unc-119(ed3)III*
OD1559	*ltSi617[pOD1592/pMMB1-1; pbub1::bub1 recoded exon5/6::bub1 3′UTR; cb-unc-119(+)]I; ltSi608[pOD1583/pMM30; pmdf-1::GFP::mdf1::mdf-1 3′UTR; cb-unc-119(+)]II; unc-119(ed3)?III; ltIs37 [pAA64; pie-1/mCHERRY::his-58; unc-119 (+)]IV; mdf-1(gk2)V*
OD1560	*ltSi629[pOD1604/pMM27; pbub1::bub1 recoded exon5/6(K718R;D847N)::bub1 3′UTR; cb-unc-119(+)]I; ltSi608[pOD1583/pMM30; pmdf-1::GFP::mdf1::mdf-1 3′UTR; cb-unc-119(+)]II; unc-119(ed3)?III; ltIs37 [pAA64; pie-1/mCHERRY::his-58; unc-119 (+)]IV; mdf-1(gk2)V*

Table S1. ***C. elegans* strains used in this study** *(Continued)*

Strain number	Genotype
OD1561	*ltSi628[pOD1603/pMM2; pbub1::bub1 recoded exon5/6(D814N)::bub1 3′UTR; cb-unc-119(+)]I; ltSi608[pOD1583/pMM30; pmdf-1::GFP::mdf1::mdf-1 3′UTR; cb-unc-119(+)]II; unc-119(ed3)?III; ltIs37 [pAA64; pie-1/mCHERRY::his-58; unc-119 (+)]IV; mdf-1(gk2)V*
OD1629	*ltSi617[pOD1592/pMMB1-1; pbub1::bub1 recoded exon5/6::bub1 3′UTR; cb-unc-119(+)]I; ruIs32[pAZ132; Ppie-1::GFP::histone H2B; unc-119(+)]III; unc-119(ed3)?III; ltSi35[pOD1034/pRG47; Pspdl-1::SPDL-1reencoded::mCherry; cb-unc-119(+)]IV*
OD1630	*ltSi629[pOD1604/pMM27; pbub1::bub1 recoded exon5/6(K718R;D847N)::bub1 3′UTR; cb-unc-119(+)]I; ruIs32[pAZ132; Ppie-1::GFP::histone H2B; unc-119(+)]III; unc-119(ed3)?III; ltSi35[pOD1034/pRG47; Pspdl-1::SPDL-1reencoded::mCherry; cb-unc-119(+)]IV*
OD1704	*ltSi382[pOD/pTK027; Pbub-1::Bub1 D814N reencoded; cb-unc-119(+)]II; unc-119(ed3)?III; ruIs32[pAZ132; pie-1/GFP::histone H2B]III; ddIs6 [GFP::tbg-1; unc-119(+)]V*
OD1748	*ltSi161[pDC117;Phim-10:HIM-10 reencoded::-mCherry; cb-unc-119(+)]II #1; unc-119(ed3)?III; him-10(ok263)III*
OD1761	*ltSi633[pOD1608/pMM34-CC; pbub1::bub1 recoded exon5/6(L777K;N781K)::bub1 3′UTR; cb-unc-119(+)]I; unc-119(ed3)III;*
OD1763	*ltSi633[pOD1608/pMM34-CC; pbub1::bub1 recoded exon5/6(L777K;N781K)::bub1 3′UTR; cb-unc-119(+)]I; ltSi608[pOD1583/pMM30; pmdf-1::GFP::mdf1::mdf-1 3′UTR; cb-unc-119(+)]II; unc-119(ed3)?III; ltIs37 [pAA64; pie-1/mCHERRY::his-58; unc-119 (+)]IV; mdf-1(gk2)V*
OD1774	*ltSi261[pTK009 Pknl-1::KNL-1reencoded(Mutant (D241–505)::RFP; cb-unc-119(+)]II; unc-119(ed3)?III; unc-46 mdf-1(gk2)V; jzIs1[pRK139; Ppie-1::GFP::mdf-1 unc-119(+)]*
OD1968	*ltSi617[pOD1592/pMMB1-1; pbub1::bub1 recoded exon5/6::bub1 3′UTR; cb-unc-119(+)]I; unc-119(ed3)?III; ruIs32[pAZ132; pie-1/GFP::histone H2B]III; ddIs6 [GFP::tbg-1; unc-119(+)]V*
OD1969	*ltSi633[pOD1608/pMM34-CC; pbub1::bub1 recoded exon5/6(L777K;N781K)::bub1 3′UTR; cb-unc-119(+)]I; unc-119(ed3)?III; ruIs32[pAZ132; pie-1/GFP::histone H2B]III; ddIs6 [GFP::tbg-1; unc-119(+)]V*
TH32	*unc-119(ed3)III; ruIs32[pAZ132; pie-1/GFP::histone H2B]III; ddIs6 [GFP::tbg-1; unc-119(+)]V*

ddIs68 [bub-1::TY1::EGFP::3xFLAG(92C12) + unc-119(+)] was a gift from M. Sarov and A. Hyman (Max Planck Institute for Cell Biology and Genetics, Dresden, Germany), and *jzIs1[pRK139; Ppie-1::GFP::mdf-1 unc-119(+)]* was a gift from R. Kitagawa (Nationwide Children's Hospital, Columbus, OH).

Table S2. **Oligos and templates used for dsRNA production**

Gene	Oligonucleotide 1 (5′ → 3′)	Oligonucleotide 2 (5′ → 3′)	Template	Concentration
				mg/ml
zyg-1 (F59E12.2)	AATTAACCCTCACTAAAGGTGGACGG AAATTCAAACGAT	TAATACGACTCACTATAGGAACGAAAT TCCCTTGAGCTG	N2 genomic	3.6–1.4
bub-1 (R06C7.8)	AATTAACCCTCACTAAAGGCCTCATTGA ACTTGGAAACC	TAATACGACTCACTATAGGGATCCGAA TTGGCACATAA	N2 genomic	2–1.6
knl-1 (C02F5.1)	AATTAACCCTCACTAAAGGAATCTCGAA TCACCGAAATGTC	TAATACGACTCACTATAGGTTCACAAA CTTGGAAGCCGCTG	N2 cDNA	3.9–1.5
rod-1 (F55G1.4)	AATTAACCCTCACTAAAGGAATGCAAAT CTTTTTGGATGGGAGAAAC	TAATACGACTCACTATAGGCATCGACG AATTTGATTCGATCAATC	N2 cDNA	2.5
ndc-80 (W01B6.9)	AATTAACCCTCACTAAAGGTGGATGAC AAGTACATTCAGAGATTATAC	TAATACGACTCACTATAGGACGATCCA ACTCGCTTTGAATTTCC	N2 cDNA	2
mdf-1 (mad-1) (C50F4.11)	AATTAACCCTCACTAAAGGCAATACAA ACTTGCCGGAAC	TAATACGACTCACTATAGGCATTGACA GAATCACTCAGCTC	N2 cDNA	2.8
mdf-2 (mad-2) (Y69A2AR.30)	AATTAACCCTCACTAAAGGGTGAACTG ACGTCGAGAATGAG	TAATACGACTCACTATAGGGACGGAT GTAAAGACACAAAACG	N2 genomic	4.4

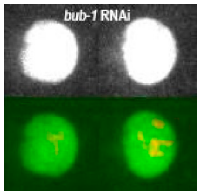

Video 1. **MAD-1 localization to unattached kinetochores requires BUB-1.** Video shows GFP::MAD-1 and mCh::H2b in two-cell *C. elegans* embryos undergoing monopolar mitosis after ZYG-1 depletion. Images were acquired using a spinning-disk confocal system (Revolution XD; Andor Technology). Two different sequences are shown for each condition. The images in the video from left to right show control (*zyg-1 RNAi*) and *bub-1 + zyg1 RNAi*. Top images are GFP::MAD-1; bottom images are a merge of GFP::MAD-1 and mCh::H2b. Frame seven is when pseudometaphase plate formation occurs. Each frame in the video is 15 s apart and is a maximum intensity projection of 6 × 2–µm z sections. Playback rate is six frames per second (90× real time). Images in the related figure (Fig. 2 A) are taken from the first sequence shown for each condition.

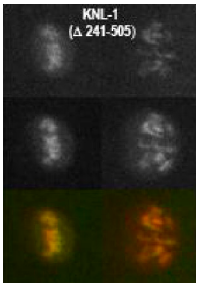

Video 2. **BUB-1 localization to kinetochores requires repetitive segments in the KNL-1 N terminus.** Video shows BUB-1::GFP and KNL-1::mCh variants in two-cell *C. elegans* embryos depleted of endogenous KNL-1 and undergoing monopolar mitosis caused by ZYG-1 depletion. Images were acquired using a spinning-disk confocal system (Andor Revolution XD; Andor Technology). Two different sequences are shown for each condition. The images in the video from left to right show KNL-1::mCh (WT), KNL-1::mCh (Δ241–505), and KNL-1::mCh (Δ85–505). Images in top row are BUB-1::GFP; middle row images are KNL-1::mCh variants; bottom row images are a color merge. Frame seven is when pseudometaphase plate formation occurs. Each frame in the video is 15 s apart and is a maximum intensity projection of 6 × 2–µm z sections. Playback rate is six frames per second (90× real time). Images in the related figure (Fig. 2 C) are taken from the first sequence shown for each condition.

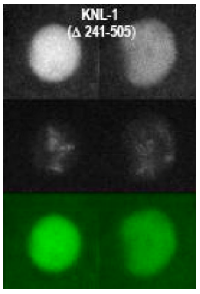

Video 3. **MAD-1 localization to unattached kinetochores requires repetitive segments in the KNL-1 N terminus.** Video shows GFP::MAD-1 and KNL-1::mCh variants in two-cell *C. elegans* embryos depleted of endogenous KNL-1 and undergoing monopolar mitosis caused by ZYG-1 depletion. Images were acquired using a spinning-disk confocal system (Andor Revolution XD; Andor Technology). Two different sequences are shown for each condition. The images in the video from left to right show KNL-1::mCh (WT), KNL-1::mCh (Δ241–505), and KNL-1::mCh (Δ85–505). Top row images are GFP::MAD-1, middle row images are KNL-1::mCh variants, and bottom row images are a color merge. Frame seven is when pseudometaphase plate formation occurs. Each frame in the video is 15 s apart and is a maximum intensity projection of 6 × 2–µm z sections. Playback rate is six frames per second (90× real time). Images in the related figure (Fig. 2 C) are taken from the first sequence shown for each condition.

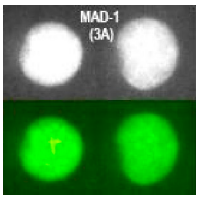

Video 4. **BUB-1 interaction-defective MAD-1 mutants are compromised in their ability to localize to unattached kinetochores.** Video shows GFP::MAD-1 variants and mCh::H2b in two-cell *C. elegans* embryos undergoing monopolar mitosis after ZYG-1 depletion. Images were acquired using a spinning-disk confocal system (Andor Revolution XD; Andor Technology). Two different sequences are shown for each condition. The images in the video from left to right show GFP::MAD-1 (WT), GFP::MAD-1 (D423A), GFP::MAD-1 (3A), and GFP::MAD-1 (P504A). Top row images are GFP::MAD-1 variants; bottom row images are a merge of GFP::MAD-1 (green) and mCh::H2b (red). Frame seven is when pseudometaphase plate formation occurs. Each frame in the video is 15 s apart and is a maximum intensity projection of 6 × 2–µm z sections. Playback rate is six frames per second (90× real time). WT is the same as in Video 1, but the order of the two sequences is switched. Images in the related figure (Fig. 4 B) are taken from the first sequence shown for each condition.

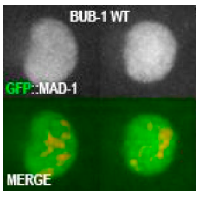

Video 5. **Alterations in the BUB-1 kinase domain perturb MAD-1 localization to unattached kinetochores independently of kinase activity.** Video shows GFP::MAD-1 and mCh::H2b in two-cell *C. elegans* embryos expressing untagged BUB-1 variants and depleted of endogenous BUB-1, which are undergoing monopolar division caused by ZYG-1 depletion. Images were acquired using a spinning-disk confocal system (Andor Revolution XD; Andor Technology). Two different sequences are shown for each condition. The images in the video from left to right show BUB-1 (WT), BUB-1 (L777K, N781K), BUB-1 (K718R, D847N), and BUB-1 (D814N). Top row images are GFP::MAD-1; bottom row images are a merge of GFP::MAD-1 (green) and mCh::H2b (red). Frame seven is when pseudometaphase plate formation occurs. Each frame in the video is 15 s apart and is a maximum intensity projection of 6 × 2–µm z sections. Playback rate is six frames per second (90× real time). Images in the related figure (Fig. 5 D) are taken from the first sequence shown for each condition.

References

Cheerambathur, D.K., R. Gassmann, B. Cook, K. Oegema, and A. Desai. 2013. Crosstalk between microtubule attachment complexes ensures accurate chromosome segregation. *Science*. 342:1239–1242. http://dx.doi.org/10.1126/science.1246232

Espeut, J., D.K. Cheerambathur, L. Krenning, K. Oegema, and A. Desai. 2012. Microtubule binding by KNL-1 contributes to spindle checkpoint silencing at the kinetochore. *J. Cell Biol.* 196:469–482. http://dx.doi.org/10.1083/jcb.201111107

Essex, A., A. Dammermann, L. Lewellyn, K. Oegema, and A. Desai. 2009. Systematic analysis in *Caenorhabditis elegans* reveals that the spindle checkpoint is composed of two largely independent branches. *Mol. Biol. Cell*. 20:1252–1267. http://dx.doi.org/10.1091/mbc.E08-10-1047

McDonnell, A.V., T. Jiang, A.E. Keating, and B. Berger. 2006. Paircoil2: improved prediction of coiled coils from sequence. *Bioinformatics*. 22:356–358. http://dx.doi.org/10.1093/bioinformatics/bti797

Notredame, C., D.G. Higgins, and J. Heringa. 2000. T-Coffee: A novel method for fast and accurate multiple sequence alignment. *J. Mol. Biol.* 302:205–217. http://dx.doi.org/10.1006/jmbi.2000.4042

O'Connell, K.F., C. Caron, K.R. Kopish, D.D. Hurd, K.J. Kemphues, Y. Li, and J.G. White. 2001. The *C. elegans* zyg-1 gene encodes a regulator of centrosome duplication with distinct maternal and paternal roles in the embryo. *Cell*. 105:547–558. http://dx.doi.org/10.1016/S0092-8674(01)00338-5

Waterhouse, A.M., J.B. Procter, D.M. Martin, M. Clamp, and G.J. Barton. 2009. Jalview Version 2—a multiple sequence alignment editor and analysis workbench. *Bioinformatics*. 25:1189–1191. http://dx.doi.org/10.1093/bioinformatics/btp033